Available online at www.sciencedirect.com
SCIENCE DIRECT®
PERGAMON
Polyhedron 22 (2003) 2067–2076
POLYHEDRON
www.elsevier.com/locate/poly

Hybrid density-functional theory studies on stable polycarbenes

Mitsuo Shoji, Takeshi Taniguchi, Takashi Kawakami, Kizashi Yamaguchi *

Department of Chemistry, Graduate School of Science, Osaka University, Toyonaka, Osaka 560-0043, Japan

Received 6 October 2002; accepted 17 February 2003

Abstract

Stable carbene:bis(9-(10-phenyl)anthryl)carbene and model carbenes of which have been investigated by ab initio MO and Crystal orbital calculations. By hybrid density-functional calculation (B3LYP/4-31G) the carbene has character as a triplet carbene than a triplet diradical. Based on calculations on this carbene, a polycarbene is contrived to investigate interactions of carbenes, which are stabilized by aromatic rings. They have interacted with each other in antiferromagnetic fashion by both B3LYP MO and Crystal orbital calculations. Their magnetic interactions have been varied as the conformational changes of the aromatic rings, which have been evaluated by the effective exchange integral J(AP) based on the Heisenberg Hamiltonian. To describe the behavior AO-approach has been introduced and has worked efficiently.

Keywords: Bis(9-(10-phenyl)anthryl)carbene; Polycarbene; Ab initio method; Effective exchange integral; AO-fitting; AO-approach

1. Introduction

The triplet bis(9-(10-phenyl)anthryl)carbene **1** synthesized by Tomioka et al. [1] was reported as very stable molecules and half-life time at room temperature is 19 min. Electron paramagnetic resonance (EPR) signals indicated the carbene structure and state of unpaired electrons. The terminal phenyl groups were not in the same planes as anthryl rings and unpaired electrons were delocalized over to C_{10} position of the anthryl rings. The carbene was like a triplet carbene rather than triplet diradical from E value of the EPR zero-field splitting parameters, reaction with oxygen to form the corresponding ketones and main decay path to form dimer through coupling of two molecules at their carbene centers [1].

In the present work, we have studied electronic and magnetic properties of **1** by unesticted Hartree-Fock (UHF) and broken-symmetry hybrid density-functional theory (UB3LYP) calculations. The magnetic property has been evaluated in terms of the energy gap between the high-spin (HS) and low-spin (LS) states. We focused upon spin distributions whether **1** is like a triplet carbene or triplet diradical. Moreover, referring to the results of **1**, we introduced some models **1a**–**5a** of polycarbene whose triplet carbenes are stabilized by next phenyl rings. For these models, we investigated magnetic interactions and spin distributions as the variation of dihedral angle between two phenyl rings. The magnetic interaction was evaluated with the effective exchange integral J based on Heisenberg Hamiltonian. To describe the dihedral angle behaviors of the effective exchange integral two sites model system which has only two p-orbitals and two electrons, has been studied and adapted to the, models **2a**, **3a**, **4a** which have MOs. This atomic orbital (AO)-approach can be used for interpolation purpose from values at two different

* Corresponding author. Tel.: +81-6-6850-5405; fax: +81-6-6850-5550.
E-mail address: yama@chem.sci.osaka-u.ac.jp (K. Yamaguchi).

0277-5387/03/$ - see front matter
doi:10.1016/S0277-5387(03)00209-2

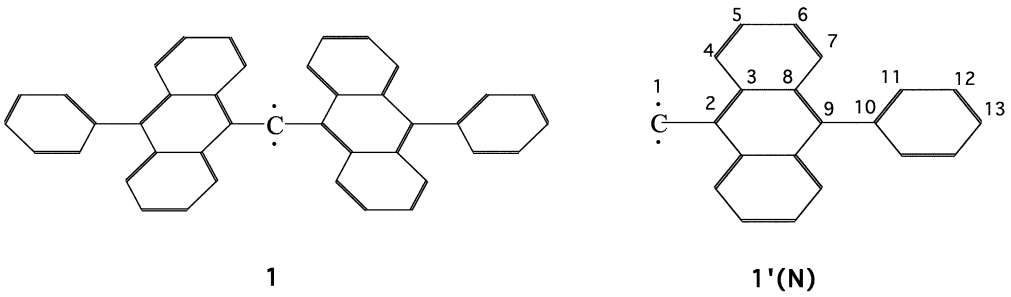

Fig. 1. Structures of stable triplet carbene; bis(9-(10-phenyl)anthryl)carbene **1**. Atomic site indices of **1** are illustrated in **1′**, in which only one part of the molecule is shown for clarity. Indices from 1 to 13 are for carbon.

conformations. AO-fitting curves reproduced the characteristic J value behaviors of ab initio calculations.

2. Theoretical backgrounds

2.1. Models: molecules and a polymer

The molecular structure of **1** is shown in Fig. 1. Rotation angles between anthryl rings and the phenyl rings are 90° and dihedral angles among the nearest aromatic rings are also 90°. In polycarbene **5a**, which is depicted in Fig. 2, there are two units which have perpendicularly oriented phenyl rings at both sides of the carbene and a variable dihedral angle (θ) is formed by the two phenyl rings between the carbenes. Model carbene **1a** is corresponding to the unit but dihedral angle defined by the phenyl rings connecting both sides of carbene center is variable. Model carbene **2a** is one part of the polycarbene **5a**, which has two methyl radicals. Variable angle of this carbene **2a** is defined by two phenyl rings where the phenyl ring and methyl

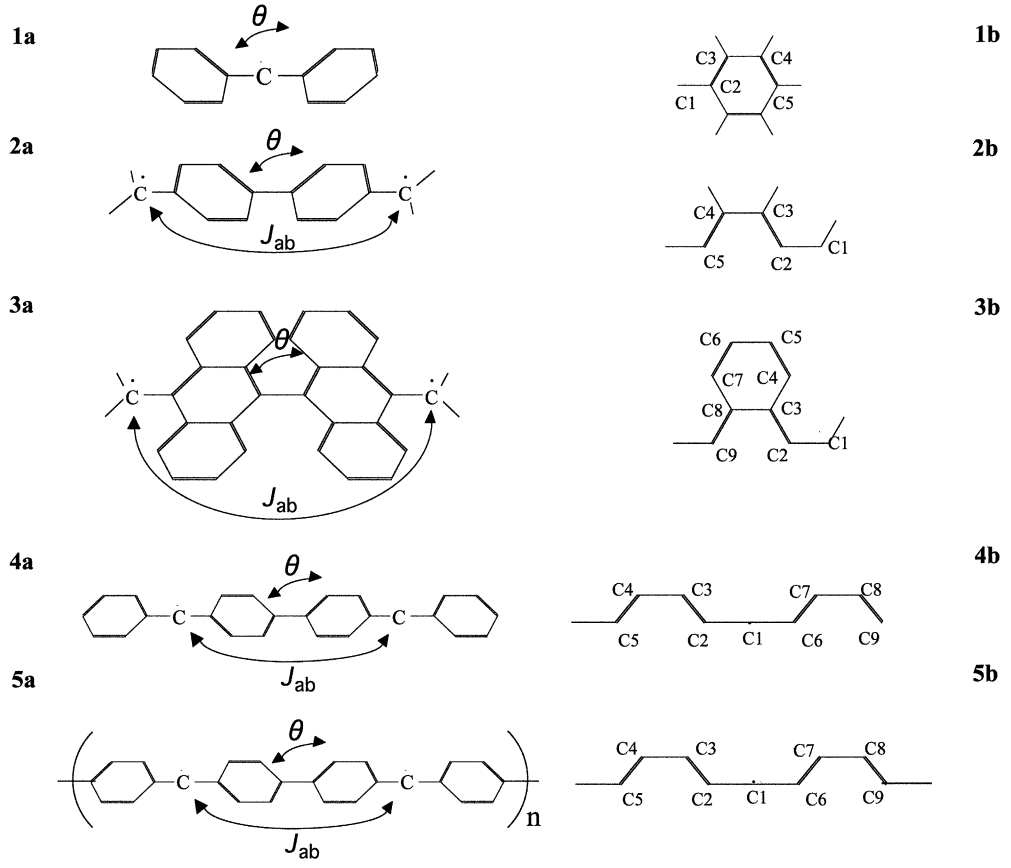

Fig. 2. Structures of molecules **1a**–**4a** and polymer **5a**. **1b**–**5b** illustrates atomic site indices of **1a**–**5a**, in which only one part of the polymer or molecule are shown for clarity.

radical are fixed on the same plane during our study. Model carbene **3a** is modified molecule of **2a**, in which the phenyl groups are replaced with anthryl groups. Model carbene **4a** is a monomer of **5a** with hydrogen atoms at both ends. Variable angle (θ) is the same as in the case of **5a**. All the models consist of standard parameters for bond length; C–C = 1.4 Å and C–H = 1.1 Å, C–C–C bond angles: 120° and linear carbine bond angles: 180°. Both HS and LS states are calculated in all carbenes **1**, **1a**–**5a** and in model carbenes **1a**–**5a** calculations are performed with changing their variable dihedral angles.

2.2. Effective exchange integrals

The effective exchange interactions between magnetic sites in HS or LS polyradicals have been described by an isotropic spin Hamiltonian model, the Heisenberg model (HB),

$$H(\mathrm{HB}) = -2\sum J_{\mathrm{ab}}\mathbf{S}_{\mathrm{a}}\mathbf{S}_{\mathrm{b}} \tag{1}$$

where $\mathbf{S}_{\mathrm{a}}$ and $\mathbf{S}_{\mathrm{b}}$ represent spins at sites a and b, respectively [2]. J_{ab} is the effective exchange integral, which can be experimentally determined by the measurement of magnetic susceptibility and so on. When HB in Eq. (1) is applied to magnetic materials, a spin projection should be carried out because spin contaminations occur in the spin-polarized DFT and UHF methods. J_{ab} values are estimated from the approximate spin projection (AP) procedure [3];

$$J_{\mathrm{ab}}(\mathrm{AP-x}) = \frac{E_{\mathrm{x}}^{\mathrm{LS}} - E_{\mathrm{x}}^{\mathrm{HS}}}{\langle S^2\rangle_{\mathrm{x}}^{\mathrm{HS}} - \langle S^2\rangle_{\mathrm{x}}^{\mathrm{LS}}} \tag{2}$$

where $\langle S^2\rangle$ is the expectation value of squared magnitudes of spin angular momentums and subscript x means calculation methods such as HF and DFT.

We calculated the S–T gap as

$$\Delta E_{\mathrm{x}} = E_{\mathrm{x}}(\mathrm{Singlet}) - E_{\mathrm{x}}(\mathrm{Triplet}) \tag{3}$$

When singlet states are calculated using unrestricted spin orbitals, the singlet states are spin contaminating with higher spin states. In the other words, singlet states are not pure singlet states such as having no-zero $\langle S^2\rangle$ expectation values. To approximately evaluate LS state energy, AP scheme of two sites model are used [3] as

$$E_{\mathrm{x}}^{\mathrm{AP-LS}}X = E^{\mathrm{LS}} + J(\mathrm{AP-x})\langle S^2\rangle^{\mathrm{LS}} \tag{4}$$

2.3. AO-fitting approach

The AO-fitting approach: a theoretical approach based on AO, are introduced as follows. Consider simple systems which have only two sites (1,2) along x axis. Each site has one p-orbital containing one electron. In HS state each site contains one α electron, though in LS state one site contains one α electron and another has one β electron. In parallel (P) system, the p-orbitals are oriented in parallel and its parallel magnetic interaction is noted as J_{P}. In orthogonal (O) system, p-orbitals are oriented in orthogonal and its orthogonal magnetic interaction is noted as J_{O}. Applying H(HB) to these systems, the total energy of HS and LS can be calculated as below: for the HS state on the system P,

$$\langle H(\mathrm{HB})\rangle_{\mathrm{P}}^{\mathrm{HS}} = -\frac{1}{2}J_{\mathrm{P}}, \quad \langle S^2\rangle_{\mathrm{P}}^{\mathrm{HS}} = 2 \tag{5}$$

and for the LS state,

$$\langle H(\mathrm{HB})\rangle_{\mathrm{P}}^{\mathrm{LS}} = \frac{1}{2}J_{\mathrm{P}} + J_{\mathrm{P}}\langle \mathrm{p}_z^1|\mathrm{p}_z^2\rangle^2, \quad \langle S^2\rangle_{\mathrm{P}}^{\mathrm{LS}} = 1 - \langle \mathrm{p}_z^1|\mathrm{p}_z^2\rangle^2 \tag{6}$$

where the superscript m of p_n^m mean the site index.

For the system O, these values are given by respectively,

$$\langle H(\mathrm{HB})\rangle_{\mathrm{O}}^{\mathrm{HS}} = -\frac{1}{2}J_{\mathrm{O}}, \quad \langle S^2\rangle_{\mathrm{O}}^{\mathrm{HS}} = 2 \tag{7}$$

$$\langle H(\mathrm{HB})\rangle_{\mathrm{O}}^{\mathrm{LS}} = \frac{1}{2}J_{\mathrm{O}}, \quad \langle S^2\rangle_{\mathrm{O}}^{\mathrm{LS}} = 1 \tag{8}$$

On the system O, orbital overlap of p_z^1 and p_y^2 are zero due to its orthogonality orientation.

Next, we consider a rotated (R) system, where p-orbital of site 2 is rotated from p_z-orbital around the x axis by θ. In this system R, an expectation value of an operator A is evaluated as

$$\langle A\rangle = \langle \mathrm{p}_z^1\mathrm{p}^2|A|\mathrm{p}_z^1\mathrm{p}^2\rangle \tag{9a}$$

$$\langle A\rangle = \langle \mathrm{p}_z^1(\mathrm{p}_z^2\cos\theta + \mathrm{p}_y^2\sin\theta)|A|\mathrm{p}_z^1(\mathrm{p}_z^2\cos\theta + \mathrm{p}_y^2\sin\theta)\rangle \tag{9b}$$

$$\langle A\rangle = \langle \mathrm{p}_z^1\mathrm{p}_z^2|A|\mathrm{p}_z^1\mathrm{p}_z^2\rangle\cos^2\theta + \langle \mathrm{p}_z^1\mathrm{p}_y^2|A|\mathrm{p}_z^1\mathrm{p}_z^2\rangle\cos\theta\sin\theta + \langle \mathrm{p}_z^1\mathrm{p}_z^2|A|\mathrm{p}_z^1\mathrm{p}_y^2\rangle\sin\theta\cos\theta + \langle \mathrm{p}_z^1\mathrm{p}_y^2|A|\mathrm{p}_z^1\mathrm{p}_y^2\rangle\sin^2\theta \tag{9c}$$

If the operator A has only one particle interactions, then

$$\langle A\rangle = \langle \mathrm{p}_z^1\mathrm{p}_z^2|A|\mathrm{p}_z^1\mathrm{p}_z^2\rangle\cos^2\theta + \langle \mathrm{p}_z^1\mathrm{p}_y^2|A|\mathrm{p}_z^1\mathrm{p}_y^2\rangle\sin^2\theta \tag{10a}$$

$$\langle A\rangle = \langle A\rangle_0\cos^2\theta + \langle A\rangle_{90}\sin^2\theta \tag{10b}$$

Since S^2 and Heisenberg Hamiltonian have only one particle interactions, above Eq. (10b) can be applied to evaluate expectation values. The gap between HS state and LS state of $\langle A\rangle$ value: $\langle A\rangle^{\mathrm{HS-LS}}$ can be reproduced as

$$\langle S^2\rangle_{\theta}^{\mathrm{HS-LS}} = \langle S^2\rangle_{\mathrm{P}}^{\mathrm{HS-LS}}\cos^2\theta + \langle S^2\rangle_{\mathrm{O}}^{\mathrm{HS-LS}}\sin^2\theta \tag{11a}$$

$$\langle H(\mathrm{HB})\rangle_\theta^{\mathrm{HS-LS}} = \langle H(\mathrm{HB})\rangle_\mathrm{P}^{\mathrm{HS-LS}} \cos^2\theta + \langle H(\mathrm{HB})\rangle_\mathrm{O}^{\mathrm{HS-LS}} \sin^2\theta \tag{11b}$$

or

$$\langle S^2\rangle_\theta^{\mathrm{HS-LS}} = \langle S^2\rangle_\mathrm{P}^{\mathrm{HS-LS}} + (\langle S^2\rangle_\mathrm{O}^{\mathrm{HS-LS}} - \langle S^2\rangle_\mathrm{P}^{\mathrm{HS-LS}}) \sin^2\theta \tag{11c}$$

$$\langle H(\mathrm{HB})\rangle_\theta^{\mathrm{HS-LS}} = \langle H(\mathrm{HB})\rangle_\mathrm{P}^{\mathrm{HS-LS}} + (\langle H(\mathrm{HB})\rangle_\mathrm{O}^{\mathrm{HS-LS}} - \langle H(\mathrm{HB})\rangle_\mathrm{P}^{\mathrm{HS-LS}})\sin^2\theta \tag{11d}$$

where

$$\langle H(\mathrm{HB})\rangle^{\mathrm{HS-LS}} = \langle H(\mathrm{HB})\rangle^{\mathrm{HS}} - \langle H(\mathrm{HB})\rangle^{\mathrm{LS}} \tag{12a}$$

$$\langle S^2\rangle^{\mathrm{HS-LS}} = \langle S^2\rangle^{\mathrm{HS}} - \langle S^2\rangle^{\mathrm{LS}} \tag{12b}$$

In the system R, energy gaps and difference of $\langle S^2\rangle$ value between HS state and LS state are as follows

$$\langle S^2\rangle_\theta^{\mathrm{HS-LS}} = 1 + \langle \mathrm{p}_z^1|\mathrm{p}_z^2\rangle^2 \cos^2\theta \tag{13a}$$

$$= \langle H(\mathrm{HB})\rangle_\mathrm{P}^{\mathrm{HS-LS}} \cos^2\theta + \langle H(\mathrm{HB})\rangle_\mathrm{O}^{\mathrm{HS-LS}} \sin^2\theta \tag{13b}$$

$$= -J_\mathrm{P}(1 + \langle \mathrm{p}_z^1|\mathrm{p}_z^2\rangle^2) \cos^2\theta - J_\mathrm{O} \sin^2\theta \tag{13c}$$

$$= (J_\mathrm{P} - J_\mathrm{O}) \sin^2\theta - J_\mathrm{P}\langle S^2\rangle_\theta^{\mathrm{HS-LS}} \tag{13d}$$

and J(AP) value of Eq. (2) is

$$J(AP)_\theta = -\frac{\langle H(\mathrm{HB})\rangle_\theta^{\mathrm{HS-LS}}}{\langle S^2\rangle_\theta^{\mathrm{HS-LS}}} = -\frac{(J_\mathrm{P} - J_\mathrm{O})\sin^2\theta - J_\mathrm{P}\langle S^2\rangle_\theta^{\mathrm{HS-LS}}}{\langle S^2\rangle_\theta^{\mathrm{HS-LS}}} \tag{14}$$

If we set $J_\mathrm{P} = J_\mathrm{v} = J$, the above Eq. (14) is equal to J, exactly. In system R, $\langle S^2\rangle_\theta^{\mathrm{HS-LS}}$ is evaluated with Eq. (13a). Generally, Eq. (13a) can not be used for the systems having HS polalization effects or many radicals. And Eq. (14) is useless as interpolation purpose for necessaries of $\langle S^2\rangle_\theta^{\mathrm{HS-LS}}$. On the other hand, it is useful to apply Eq. (11a) or Eq. (11b) for general systems. Using these equations, J(AP) value can be estimated as

$$J(AP)' = -\frac{\langle H(\mathrm{HB})\rangle_\theta^{\mathrm{HS-LS}}}{\langle S^2\rangle_\theta^{\mathrm{HS-LS}}} \tag{15}$$

from P and O orientation results using Eq. (11a) or Eq. (11b). Estimation values in other angle θ can be evaluated using estimation values in two other angles (θ_1, θ_2) as

$$\langle A\rangle_\theta = \frac{\langle A\rangle_{\theta_1}(\sin^2\theta_2 - \sin^2\theta) - \langle A\rangle_{\theta_2}(\sin^2\theta_1 - \sin^2\theta)}{\sin^2\theta_2 - \sin^2\theta_1} \tag{16a}$$

or

$$\langle A\rangle_\theta = \frac{\langle A\rangle_{\theta_1}\sin^2\theta_2 - \langle A\rangle_{\theta_2}\sin^2\theta_1 - (\langle A\rangle_{\theta_1} - \langle A\rangle_{\theta_2})\sin^2\theta}{\sin^2\theta_2 - \sin^2\theta_1} \tag{16b}$$

which are generalized ones of Eq. (10b).

Using above equation, $J(\mathrm{AP})_\theta$ can also be estimated from $\langle S^2\rangle_\theta^{\mathrm{HS-LS}}$ and $E^{\mathrm{HS-LS}}$ results at two different dihedral angles. We applied Eqs. (16a) and (16b)to ab initio calculation results in this study and checked the feature of Eqs. (16a) and (16b) for more realistic systems having MOs.

3. Computational procedures

1 and **1a**–**4a** molecules were carried out with GAUSSIAN-98 program packages [4]. Carbene polymer **5a** was calculated by CRYSTAL-98 program packages. We employed Pople's 4-31G basis sets [5] and tight SCF convergence criterion for all calculations of these molecules using GAUSSIAN-98 [6]. In the calculations using CRYSTAL-98 [7], we employed standard Pople 6-21G basis sets [8] for all atoms and in B3LYP calculations auxiliary basis sets of (nine s-type, two p-type and one g-type) and (12 s-type, four p-type, three d-type, two f-type and one g-type) gaussian functions [9] for hydrogen atoms and carbon atoms are employed to fit the

Table 1
Total energies (E), S^2 expectation valuse ($\langle S^2\rangle$) of high spin tryplet states and low spin singlet states and singlet–triplet energy gaps for 1

Method	High spin state (3)		Low spin state (1)		Energy gap [b]	AP-energy gap [c]
	E [a]	$\langle S^2\rangle$	E [a]	$\langle S^2\rangle$		
UHF	−1565.565257	6.8733	−1565.535610	5.5612	0.80674	4.2260
UB3LYP	−1575.903841	2.1726	−1575.898400	1.1170	0.14804	0.30469

[a] Total energies (E) are shown in a.u.
[b] Energy gap (ΔE) is defined as $\Delta E = E^{\mathrm{LS}} - E^{\mathrm{HS}}$ and given in eV.
[c] AP-energy gap ΔE^{AP} is defined as $\Delta E^{\mathrm{AP}} = E^{\mathrm{AP\text{-}LS}} - E^{\mathrm{HS}}$ and is given in eV, where $E^{\mathrm{AP-LS}}$ is purlyfied low spin state energy by Eq. (4).

exchange correlation potentials, respectively. In radial integration, the variable of points in radial quadrature reduced to 31 from default value 34 for all B3LYP calculations, because there are large number of atoms in the unit cell. The five ITOL parameters controlling the accuracy of the bielectronic Coulomb and exchange series were set as ITOL1-4 = 10 and ITOL = 20. The POLEORDR parameter, which is the maximum order of shell multipoles in the long-range zone for the electron–electron Coulomb interactions, were set as maximum value 6. The threshold variables on eigenvalues and total energies were set as eight and seven, respectively. To make spin-polarized solutions, we used CRYSTAL-98 keywords such as SPINLOCK and EIGSHIFT. In the calculation of ferromagnetic solutions, alpha electron occupancy was larger than beta one by 4 in the unit cell, i.e. we kept SPINLOCK = 4 during all SCF cycles.

4. Calculated results

4.1. Stable carbine *1*

4.1.1. S–T gap

Using Eqs. (3) and (4), spin energy gaps and AP-energy gaps are calculated, which are shown in Table 1, respectively. AP-energy gap is about twice as large as spin energy gap by UB3LYP/4-31G and about five times by UHF/4-31G. The AP-energy gap by UHF changed more largely than by UB3LYP because of high $\langle S^2 \rangle$ value in LS state. Triplet state is more stable than singlet state by 0.30 eV. In Table 1, total energy and $\langle S^2 \rangle$ by UHF and UB3LYP are also shown. UHF results have large $\langle S^2 \rangle$ in both LS and HS.

4.1.2. Spin density distributions

Table 2 list the total atomic spin density distributions on carbon atom for the carbene **1**. In this Table 2 atomic site indices are corresponding to Fig. 1 1′. These results indicate that signs of spin densities are alternating at neighboring atoms, i.e., the spin polarization effect is dominant in this molecule. The spin densities by UHF have larger amplitudes than by UB3LYP. Especially, UHF results have large spin densities further over phenyl groups due to the spin polarization effects. This agrees with having high $\langle S^2 \rangle$ in UHF. On the other hand, UB3LYP results have very small spin densities over phenyl groups also due to the spin polarization effects. That is, spin polarization is stopped by perpendicular oriented phenyl ring. In HS state the atomic spin density value in the carbene center of **1** is 1.205 which is a little larger than twice 0.491 by UB3LYP in C_{10} position of the anthryl rings which is corresponding to C9 site in Fig. 1 1′, i.e. **1** is similar to a triplet carbine than a triplet diradical, though it has

Table 2
Atomic spin density distribution on carbon atom in **1**

Method	Spin state	1	2	3	4	5	6	7	8	9	10	11	12	13
UHF	HS	2.262	−1.312	1.113	−0.949	0.912	−0.908	0.947	−1.067	1.242	−0.948	0.811	−0.778	0.780
UHF	LS	−0.001	−0.868	1.025	−0.945	0.909	−0.902	0.942	−1.057	1.244	−0.949	0.811	−0.778	0.780
UB3LYP	HS	1.205	−0.344	0.250	−0.129	0.156	−0.115	0.153	−0.180	0.491	−0.044	0.017	−0.001	0.002
UB3LYP	LS	0.000	0.167	−0.200	0.126	−0.158	0.110	−0.157	0.180	−0.518	0.047	−0.018	0.001	−0.002

triplet-diradical character. This calculation result is consistent with experimental results [1]. In addition to large atomic spin density on carbine center, atomic spin densities on C2 site and C3 site are measurable, while atomic spin densities on outer carbons (C4, C5, C6 and C7) of anthryl are small by UB3LYP. In LS state, right hand side of the carbene center and left side have opposite signed spin density distributions on the contrary in HS state. Table 2 shows only one part of **1**. In the carbene center, atomic spin density is zero. Because carbene center has opposite singed orbital spin density of 0.697 in UHF and 0.491 in UB3LYP. Each unpaired electron in carbene center is delocalized over parallel oriented anthryl π orbital.

4.2. Model *1a–5a*

4.2.1. Relative energy

Relative energies in HS states and LS states for model carbene **1a**–**5a** are given in Figs. 3–5. The zero point of the relative energy is taken from the lowest energy of θ-rotation. From the energy change for **1a** in Fig. 3 triplet HS state is more stable than singlet LS state. There are two different UHF solutions, state 1 and state 2, in LS state (Fig. 3(A)). We will discuss the difference between two LS states later in terms of spin density distributions. More stable solution is gained only in LS state by UB3LYP (Fig. 3(B)).

In molecule **2a**, singlet LS state is more stable than HS state (Fig. 4(A and B)). In other words, antiferromagnetic interaction is occurred between two radical sites. In LS state, there is stable conformation at about 40°. There would be two competitive factors. The first factor make the molecule stable, which is spin orbitals overlaps among half occupied ones. As the variable angle goes to zero, double bond is formed at center. The second factor, unstable factor is repulsions among neighboring hydrogen atoms. In HS state, repulsive curve is shown. Because the stable factor in LS state is not adaptable to the HS state. In the HS state, parallel spins can not occupy one bonding orbital by the Pauli exclusion principle. Considering above only two factors, there is no stabilizing factor in HS state. These explanations can describe UHF results qualitatively. But in HS states by UB3LYP there is stable conformation at about 40° because of electron correlation. Relative energy by UHF is about twice as large as one by UB3LYP.

The potential curve for molecule **3a** is repulsive (Fig. 4(C and D)). Repulsions between peri-hydrogen atoms are largely occupying the repulsive behavior. The calculations of low θ angles, less than 30°, had not be converged for the too many nearing of peri-hydrogen atoms.

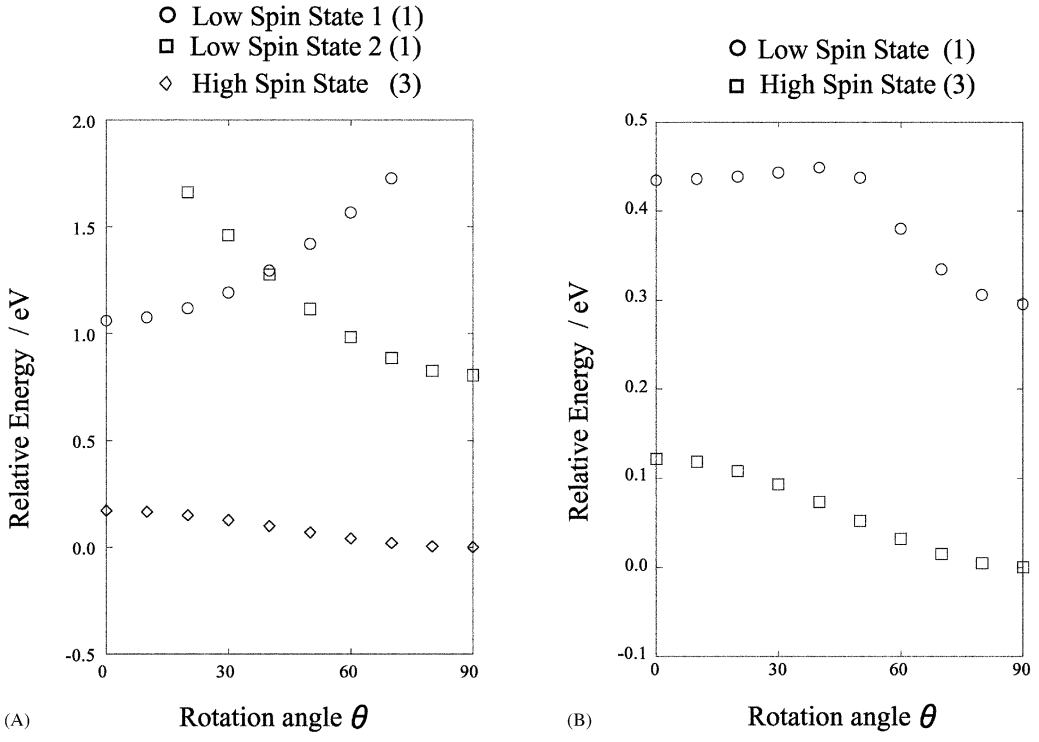

Fig. 3. Changes in relative energy of molecule **1a** under dihedral angle rotation of phenyl rings, which are both sides of carbene center. (A) and (B) are by UHF/4-31G and UB3LYP/4-31G, respectively. Spin multiplicities are given in parentheses.

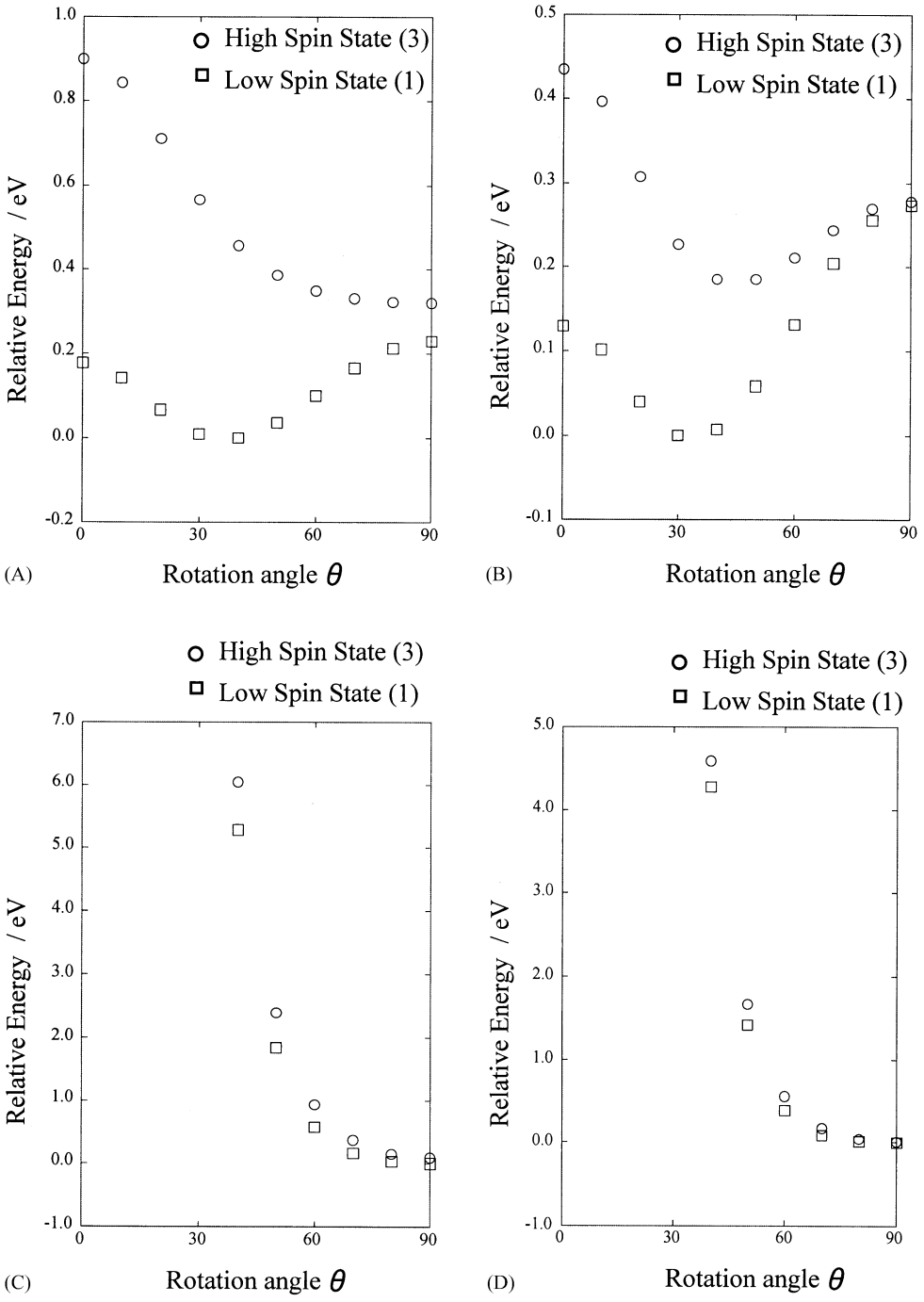

Fig. 4. Changes in relative energy of molecules **2a** and **3a** under dihedral angle rotation of phenyl rings and anthryl rings, which are among carbene centers. (A) and (B) show relative energy of **2a** by UHF/4-31G and UB3LYP/4-31G, respectively. And (C) and (D) show relative energy of **3a** by UHF/4-31G and UB3LYP/4-31G, respectively. Spin multiplicities are given in parentheses.

The energy curves of molecules **4a** and **5a** are fairly similar to **2a**'s in their shape (Fig. 5).

4.2.2. Effective exchange integral

The effective exchange integral J(AP) values and J(AP)′ curves are shown in Fig. 6. The J(AP) values using UHF are larger than UB3LYP by four times for larger S–T gap energies (Fig. 6(A and B)). J(AP)′ is interpolation curve using 0 and 90° results in **2a** and **4a** employing Eq. (15) (Fig. 6(A, B and D)). For **3a** J(AP)′ curves were gained using 40 and 90° results by additionally employing Eqs. (16a) and (16b) (Fig. 6(C)). J(AP)′ reproduce J(AP) value well, especially UB3LYP results. From the above results, the AO-fitting is

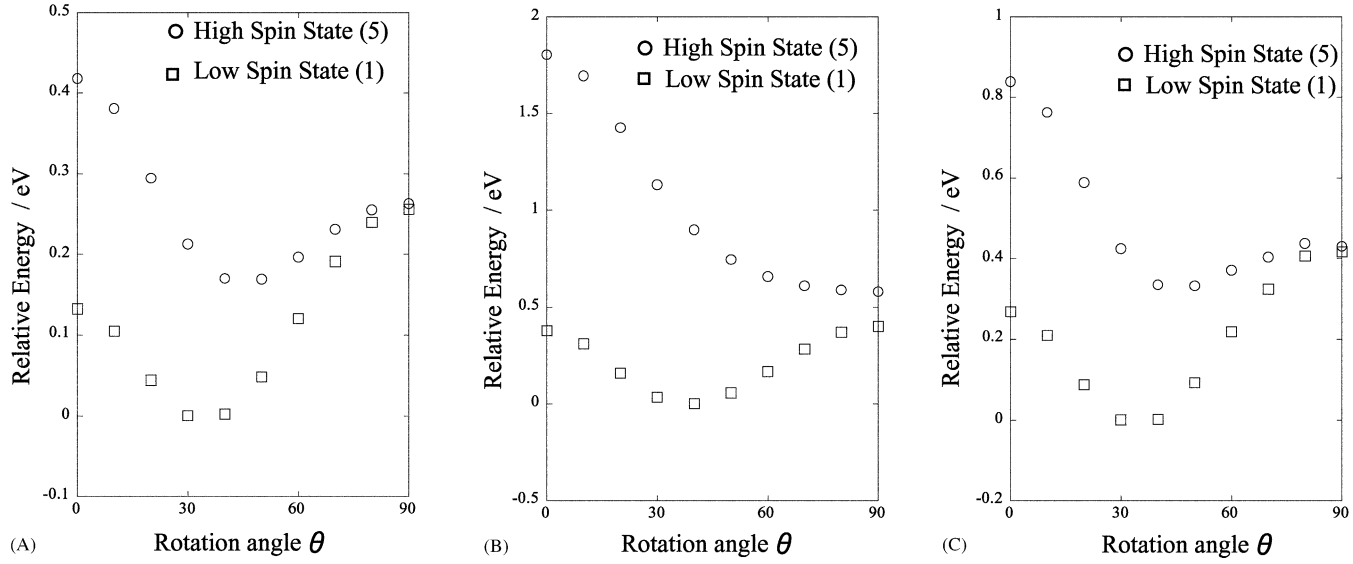

Fig. 5. Changes in relative energy of molecules **4a** and **5a** under dihedral angle rotation of monomers. (A) Show relative energy of **4a** by UB3LYP/4-31G. (B) and (C) show relative energy per Unit Cell of **5a** by UHF/6-21G and UB3LYP/6-21G, respectively. Spin multiplicities are given in parentheses.

efficient to evaluate the variation of dihedral angles. From the similarity of the J values between **2a** and **3a**, the difference between phenyl groups and anthryl groups are little. Taking into consideration of the similar energy curves between **4a** and **5a**, **5a** must have the similar J values to **4a**.

4.2.3. Spin density distributions

The total atomic spin density distributions for **1a**–**5a** are shown in Table 3. In all models and spin states, spin polarization is dominant, especially by UHF. The most largest spin densities are in carbenes for all models **1a**–**5a** and the second ones are in carbones of connecting to the next aromatic ring.

In LS state 1 for **1a**, atomic spin density distributions are symmetrical with respect to C1 site which is non-zero. On the other hand, in LS state 2, atomic spin density distributions are antisymmetrical with respect to the C1 site which is zero. Atomic spin density on C1 site is zero because spin orbital densities are same magnitude of opposite sign. Similarities in spin distributions are occurring among monomer **1a**, **4a** and polymer **5a**.

5. Discussion and conclusion

5.1. Doping of polycarbenes

Present computational results indicate that the effective exchange interaction between triplet carbene sites are antiferromagnetic in the case of *para*-bridged phenyl carbene analogs (**2a**–**5a**) examined here. This in turn means that physical and chemical dopings of these species are very interesting like cuprates, where doping of hole into antiferromagnetic CuO_2 plane is found to be the route toward high-Tc superconductivity [10]. Previously [11,12] we have examined hole and electron doping of planar biscarbenes, and found that magnetic metallic states are feasible. From this point of view, hole and/or electron doping of stable carbenes **1**–**5** seem promising to obtain functional materials with exotic electronic and magnetic properties.

5.2. Conclusion

First, from calculations for stable carbene **1**, it is found that spins on the carbene center are stabilized by spin polarization over connecting anthryl groups and are stopped by terminal phenyl groups. Investigation of the spin density distribution shows that **1** is a triplet carbene but a diradical. This is consistent with the experiment results [1]. For example, field effective transistor configuration for stable carbene polymers is such a possibility [13]. Triplet state is more stable than singlet state by 0.3 eV from approximate projection scheme. Second, studies by employing models of stable carbene give us the results as follows. The model carbene **1a** have showed that carbene is stabilized by connecting phenyl groups and triplet state is more stable than singlet state. The model carbenes **2a**–**5a** have showed that carbenes interact with each other in antiferromagnetic fashion. Tight binding orbital calculations for carbine polymer **5a** have shown the similar potential curves to molecular models'. Third the AO-approach which have introduced here for rotating of the phenyl rings bonding carbenes have worked efficiently in fitting

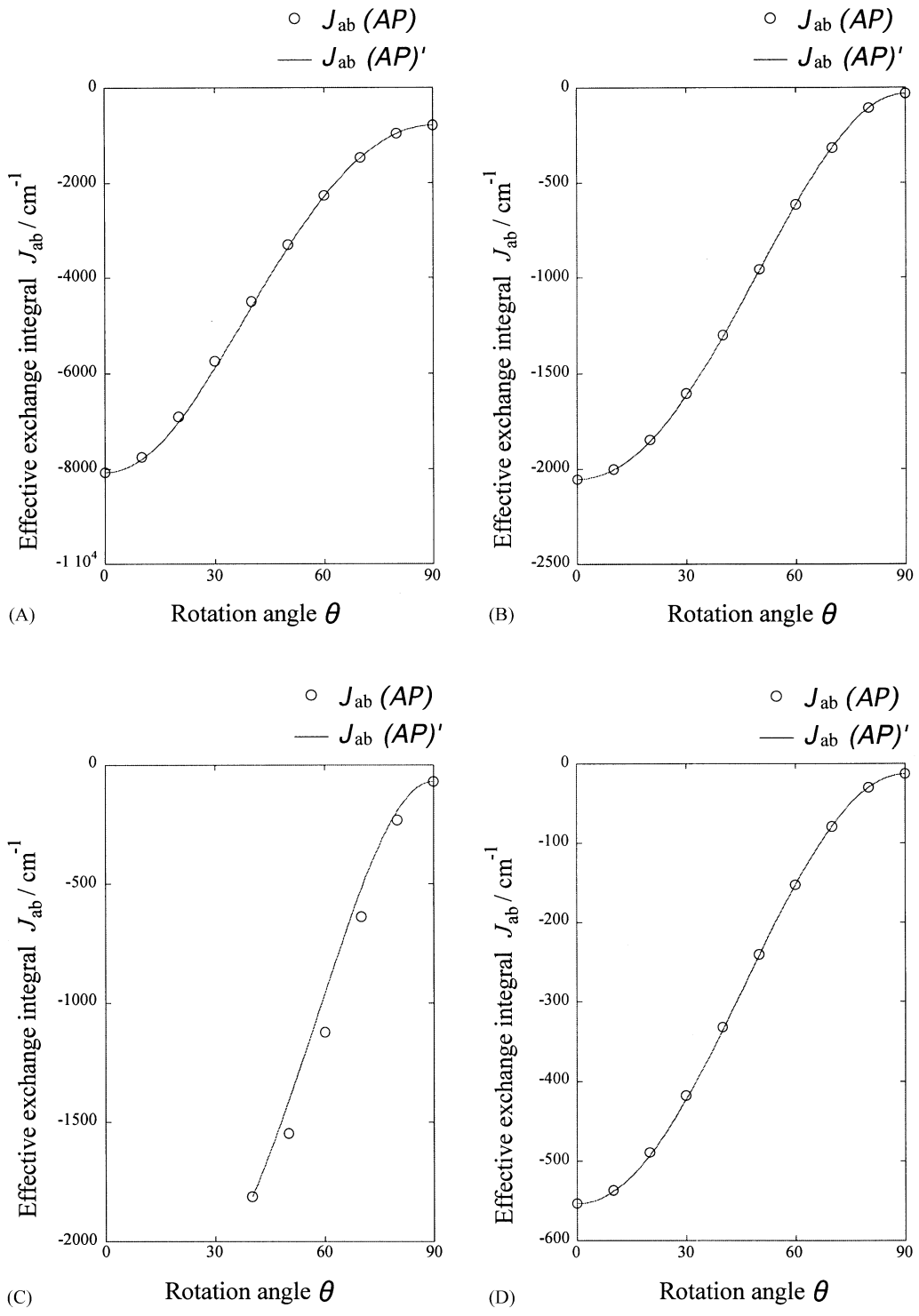

Fig. 6. J and J' values changes of molecules **2a**, **3a** and **4a** under dihedral angle rotations. (A) and (B) show J and J' values changes of **2a** by UHF/4-31G and UB3LYP/4-31G, respectively. (C) Shows J and J' values changes in **3a** by UB3LYP/4-31G. And (D) shows J and J' values changes in **4a** by UB3LYP/4-31G.

the J(AP) curves with known results at two different angles. If the polycarbene **5a** is synthesized, rotation of the connecting *para*-phenyl/anthryl groups for this polycarbene must not stabilize the ferromagnetic interactions than the antiferromagnetic interactions from this study. If ferromagnetic polycarbene is required, it must be the *meta*-polycarbene since spin polarization effect play a dominant role [11–13]. In order to make

Table 3
Atomic spin density distribution on carbon at the 90° rotated conformation

Method	Molecule	Spin state	C1	C2	C3	C4	C5	C6	C7	C8	C9
UHF	**1a**	LS1 [a]	−0.307	−0.678	0.861	−0.861	0.893				
UHF		LS2	0.000	−0.722	0.907	−0.884	0.923				
UHF		HS	2.186	−1.117	0.974	−0.884	0.914				
UB3LYP		LS1 [a]	0.489	0.063	−0.174	0.124	−0.232				
UB3LYP		LS2	0.000	0.140	−0.250	0.159	−0.293				
UB3LYP		HS	1.561	−0.313	0.294	−0.151	0.271				
UHF	**2a**	LS	−1.157	0.935	−0.947	0.911	−1.037				
UHF		HS	1.158	−0.926	0.935	−0.852	0.809				
UB3LYP		LS	−0.841	0.236	−0.266	0.160	−0.289				
UB3LYP		HS	0.842	−0.235	0.264	−0.140	0.243				
UHF	**3a**	LS	1.146	−1.086	1.073	−0.954	0.912	−0.907	0.950	−1.073	1.336
UHF		HS	1.147	−1.083	1.066	−0.952	0.912	−0.907	0.946	−1.004	1.001
UB3LYP		LS	0.622	−0.268	0.226	−0.130	0.154	−0.113	0.152	−0.194	0.564
UB3LYP		HS	0.624	−0.266	0.225	−0.129	0.153	−0.112	0.152	−0.160	0.455
UB3LYP	**4a**	LS	1.559	−0.314	0.293	−0.160	0.285	−0.313	0.293	−0.151	0.271
UB3LYP		HS	1.560	−0.312	0.291	−0.140	0.239	−0.313	0.293	−0.151	0.271
UHF	**5a**	LS	2.184	−1.094	0.945	−0.877	1.004	−1.093	0.945	−0.877	1.004
UHF		HS	1.575	−1.084	0.933	−0.816	0.776	−1.084	0.933	−0.816	0.776
UB3LYP		LS	1.578	−0.319	0.289	−0.156	0.282	−0.319	0.289	−0.156	0.282
UB3LYP		HS		−0.317	0.287	−0.136	0.236	−0.317	0.287	−0.136	0.236

[a] At the 0° rotated conformation.

ferromagnetic *para*-polycarbene, other ways such as hole doping have been under consideration with both MO and crystalline orbital approach.

Acknowledgements

This work has been supported by Grants-in-aid for Scientific Research on Priority Areas (# 14204061 and 13740396) from the Ministry of Education, Culture, Sports, Science and Technology, Japan.

References

[1] H. Tomioka, E. Iwamoto, Itakura, K. Hirai, Nature 412 (2001) 626.
[2] (a) M. Mitani, H. Mori, Y. Takano, D. Yamaki, Y. Yoshioka, K. Yamaguchi, J. Chem. Phys. 113 (2000) 4035;
(b) M. Mitani, D. Yamaki, Y. Takano, Y. Kitagawa, Y. Yoshioka, K. Yamaguchi, J. Chem. Phys. 113 (2000) 10486;
(c) M. Mitani, D. Yamaki, Y. Yoshioka, K. Yamaguchi, J. Chem. Phys. 113 (1999) 1309.
[3] Y. Takano, Y. Taniguchi, T. Isobe, H. Kubo, T. Morita, Y. Yamamoto, K. Nakasuji, T. Takui, K. Yamaguchi, J. Am. Chem. Soc. 11122 (2002) 124.
[4] GAUSSIAN 98, Revision A.6, M.J. Frisch, G.W. Trucks, H.B. Schlegel, G.E. Scuseria, M.A. Robb, J.R. Cheeseman, V.G. Zakrzewski, J.A. Montgomery Jr., R.E. Stratmann, J.C. Burant, S. Dapprich, J.M. Millam, A.D. Daniels, K.N. Kudin, M.C. Strain, O. Farkas, J. Tomasi, V. Barone, M. Cossi, R. Cammi, B. Mennucci, C. Pomelli, C. Adamo, S. Clifford, J. Ochterski, G.A. Petersson, P.Y. Ayala, Q. Cui, K. Morokuma, D.K. Malick, A.D. Rabuck, K. Raghavachari, J.B. Foresman, J. Cioslowski, J.V. Ortiz, B.B. Stefanov, G. Liu, A. Liashenko, P. Piskorz, I. Komaromi, R. Gomperts, R.L. Martin, D.J. Fox, T. Keith, M.A. Al-Laham, C.Y. Peng, A. Nanayakkara, C. Gonzalez, M. Challacombe, P.M.W. Gill, B. Johnson, W. Chen, M.W. Wong, J.L. Andres, C. Gonzalez, M. Head-Gordon, E.S. Replogle, J.A. Pople, Gaussian Inc., Pittsburgh PA, 1998.
[5] R. Ditchfield, W.J. Hehre, J.A. Pople, J. Chem. Phys. 54 (1971) 724.
[6] GAUSSIAN98 User's Reference second ed., Gaussian, Inc.
[7] CRYSTAL98 User's Manual, R. Dovesi, V.R. Saunders, C. Roetti, M. Causa, N.M. Harrison, R. Orlando, C.M. Zicovich-Wilson.
[8] D.J. Hwhre, L. Radom, P.v.R. Schleyer, J.A. Pople, Ab Initio Molecular Orbital Theory, Wiley, New York, 1986.
[9] R. Orlando et al, CRYSTAL DF Auxiliary Basis sets. Available from http://www.chimifm.unito.it/teorica/crystal/AuxB_Sets/hydrogen.html, http://www.chimifm.unito.it/teorica/crystal/AuxB_Sets/carbon.html.
[10] J.G. Bednort, K.A. Muller, Z. Phys. 64 (1986) 189.
[11] K. Yamaguchi, Y. Toyoda, T. Fueno, Synthetic Metals 19 (1987) 81.
[12] (a) S. Yamanaka, M. Okumura, H. Nagao, K. Yamaguchi, Chem. Phys. Lett. 233 (1995) 88;
(b) S. Yamanaka, T. Kawakami, M. Okumura, K. Yamaguchi, Chem. Phys. Lett. 233 (1995) 257.
[13] F. Matsuoka, Y. Yamashita, T. Kawakami, Y. Kitagawa, Y. Yoshioka, K. Yamaguchi, Polyhedron 20 (2001) 1169.